Stability analysis and model-based control in EXTRAP-T2R with time-delay compensation

Erik Olofsson, Emmanuel Witrant, Corentin Briat, Silviu-Iulian Niculescu, Per Brunsell

Stability analysis and model-based control in EXTRAP-T2R with time-delay compensation

Erik Olofsson[1], Emmanuel Witrant[2], Corentin Briat[2], Silviu-Iulian Niculescu[3] and Per Brunsell[1]

***Abstract*— In this paper, we investigate the stability problems and control issues that occur in a *reversed-field pinch* (RFP) device, EXTRAP-T2R (T2R), used for research in fusion plasma physics and general plasma (ionized gas) dynamics. The plant exhibits, among other things, magnetohydrodynamic *instabilities* known as *resistive-wall modes* (RWMs), growing on a time-scale set by a surrounding non-perfectly conducting shell. We propose a novel model that takes into account experimental constraints, such as the actuators dynamics and control latencies, which lead to a multivariable time-delay model of the system. The open-loop field-error characteristics are estimated and a stability analysis of the resulting closed-loop *delay differential equation* (DDE) emphasizes the importance of the delay effects. We then design a structurally constrained optimal PID controller by *direct eigenvalue optimization* (DEO) of this DDE. The presented results are substantially based on and compared with experimental data.**

I. INTRODUCTION

Control of magnetohydrodynamic (MHD) *instabilities* in toroidal devices for magnetic confinement is a crucial issue for thermonuclear fusion plasmas (high-temperature ionized gases) [1]. Indeed, advanced plasma confinement scenarios, as considered for the ITER experiment (a major step towards industrial fusion reactors) [2], motivate a better understanding of MHD phenomena and their regulation. The reversed-field pinch (RFP) device T2R, considered in this work, is particularly well suited for MHD studies in general (one of the main focuses of this facility) and more specifically for active control of MHD modes. Continuous research efforts have been done in this direction [3], [4], [5] based on physical approaches. We are now addressing the problem from a control-oriented point of view, highlighting impact of actuator dynamics to closed-loop stabilization.

T2R, sketched in Fig. 1(a), is a torus equipped with an equidistributed array of equally shaped 4×32 actuator saddle coils fully covering the surface outside a resistive wall (and vacuum container), and a corresponding set of 4×32 sensor saddle coils inside the wall (with 50% surface coverage). The coils inputs and outputs are subtracted pairwise in a top-down and inboard-outboard fashion, effectively implying 64 control and 64 measurement signals.

The MHD instabilities lead to non-symmetric electric currents within the plasma torus, causing perturbed magnetic fields outside of the plasma at the position of the surrounding wall. Complete stabilization would be achieved by an *ideally* conducting wall forcing the boundary magnetic field to vanish. In practice, eddy currents decay allow perturbed magnetic flux to penetrate the wall and hence the MHD instabilities to grow. To counteract this problem, the *intelligent-shell* (IS) concept [6] has been devised, to emulate the behavior of an ideally conducting wall by (decentralized) *feedback* control of external current-carrying coils. The RFP type of toroidal plasma confinement is particularly suited to study this method and stabilization of multiple independent MHD instabilities has recently been reported [5]. To emphasize the significance of IS feedback MHD-stabilization for T2R, note that the plasma is confined during $\sim 15-20\,\mathrm{ms}$ only *without* IS whereas a sustained plasma current is routinely achieved for over $90\mathrm{ms}$ *with* IS (limited by the experiment's power supply). There is a strong motivation for developing this technique also for *Tokamak* fusion devices [7] (such as JET and ITER), the configuration mainly pursued today for magnetic confinement fusion research.

The aim of this paper is to introduce and analyze a new model for describing T2R dynamics, by explicitly taking into account the sensors/actuators configuration (aliasing and additional dynamics) and the control implementation (time-delays). To the best of the authors' knowledge, no systematic study of controller gain design for T2R IS operation explicitly including such experimental conditions has been made. We develop our description of the plant from a control viewpoint and employ a fixed-structure gain synthesis approach (presently instantiated for a classic PID) for T2R IS. Controller gains are directly optimized for a closed-loop delay differential equation (DDE) model. Experimental results illustrate the performance improvements in comparison with the explorative work [3], where PID gains scans and qualitative applicability of linear models were presented.

The paper is organized as follows. First, a model describing the MHD unstable modes is introduced in section II and the delay effects on the asymptotic stability of the corresponding model are analyzed in III. The design of a control law is presented in IV, and section V is devoted to experimental results and highlights the performance improvements. Some concluding remarks end the paper.

II. MAGNETOHYDRODYNAMIC UNSTABLE MODES MODEL

The purpose of this section is threefold: first, to *outline* the unstable physics, second, to interface the corresponding model to a configuration of sensors and actuators and, finally, to introduce an appropriate DDE to be analyzed.

[1]KTH/EES Fusion Plasma Physics (Association EURATOM-VR), Stockholm, Sweden [2]UJF-INPG/GIPSA-lab, Grenoble, France and [3]CNRS/Supélec Laboratoire des Signaux et Systémes, Gif-sur-Yvette, France.

Corresponding author email: erik.olofsson@ee.kth.se

A. Resistive-wall mode physics in the reversed-field pinch

MHD theory [7], [8], [9] is the underlying physical level-of-detail employed here, a continuum description intended to capture behavior of conducting fluid matter, such as plasma gases and liquid metals. MHD effectively is a simultaneous application of Navier-Stokes' and Maxwell's equations. The system at hand is approximated by a periodic *cylinder*[1], with period $2\pi R$, R being the *major* toroidal radius, and thus reduced to the *minor* radial dimension r. The well-known MHD equations are: momentum $\rho\frac{d\mathbf{v}}{dt} = \mathbf{j}\times\mathbf{B} - \nabla p$, Ohm's law $\mathbf{E} + \mathbf{v}\times\mathbf{B} = \eta\mathbf{j}$ together with Maxwell's, continuity and the adiabatic equation of state. For *ideal* MHD [8] resistivity $\eta \to 0$. A flowless $\mathbf{v} = \mathbf{0}$ and ideal equilibrium $\mathbf{j}_0\times\mathbf{B}_0 = \nabla p_0$, $\mathbf{E}_0 = \mathbf{0}$ is solved for using a standard current-profile and pressure parameterization [10], defining a magnetic structure in the plasma region $0 < r < r_a$, the *plasma column*. A vacuum layer isolates the plasma boundary $r = r_a$ from the conducting vessel wall at $r = r_w$. This wall is modeled *thin* [11]. Region $r_w < r < +\infty$ is air. An external source is positioned at $r = r_c > r_w$ (active coils outside the shell).

Linear stability of perturbations around the nominal equilibrium is investigated by Fourier spectral decomposition $\mathbf{b}(r,t) = \sum_{mn}\mathbf{b}_{mn}(r)e^{j(t\omega+m\theta+n\phi)}$, yielding a discrete enumeration (m,n) of Fourier eigenmodes $\mathbf{b}_{mn}(r)$ with associated growth-rate $\gamma_{mn} = j\omega_{mn}$, after matching of boundary conditions. Eigenfunction first-order derivative discontinuity at $r = r_w$ determines modal growth-rate $\tau_w\gamma_{mn} = [\frac{rb_r'}{b_r}]_{r_w-}^{r_w+}$ (1(b)). These modes are the *resistive-wall modes* (RWMs), growing on the resistive time-scale set by the magnetic diffusion time τ_w.

For the magnetic confinement configuration considered in this paper, the *reversed-field pinch* (RFP), named for its characteristic toroidal field reversal near the plasma boundary, it is customary to classify eigenmodes as *resonant/non-resonant* and *internal/external*. Internal modes share helicity with the equilibrium magnetic field inside the reversal surface, while external modes are reversed in this sense. *Ideal* resonant perturbations are zeroed for $0 < r < r_s < r_a$, r_s being the resonant position, as motivated in e.g. [11]. *Resistive* resonant modes are known as *tearing modes* (TMs). They are usually treated by inserting a thin resistive layer at r_s, and they typically seed *magnetic islands* governed by nonlinear dynamics [12]. Here, only ideal MHD modes are considered, modeled by

$$\tau_{mn}\dot{b}^r_{mn} - \tau_{mn}\gamma_{mn}b^r_{mn} = M_{mn}I_{mn} = b^{r,ext}_{mn} \qquad (1)$$

where b^r_{mn} is the radial Fourier component of the perturbed field, M_{mn} and I_{mn} respectively a geometric coefficient and a fourier harmonic for the external active coil current, while τ_{mn} is the mode-specific penetration time. A *range* n of unstable modes emerge for $m = 1$ (Fig. 1(b)). For a perfectly symmetric resistive wall, RWMs are uncoupled in ideal MHD regime, and growth rates are real-valued. Experimental support for model (1) is reported in e.g. [10], [13], [4].

[1]Indeed, a good approximation for large aspect-ratio (R/r_a) devices, such as EXTRAP-T2R: $R = 1.24$m, $r_a = 0.183$m

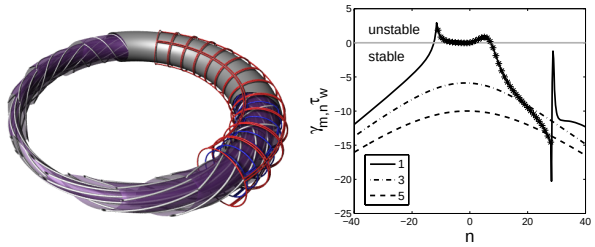

(a) Cartoon of RFP magnetic equilibrium structure, vacuum vessel, sensor (blue) and actuator (red) saddle coils.

(b) Theoretical growth-rates $\tau_w\gamma_{mn}$. Integer-n non-resonant positions (RWMs) are marked (*) for $m = 1$.

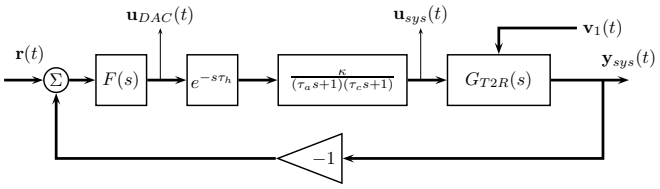

(c) Closed-loop schematics. Taps indicate available measurements.

Fig. 1. RFP device 1(a) and RWM spectrum 1(b). All signal routings 1(c) are 64 parallel channels.

B. MIMO plant modeling by geometric coupling of SISO dynamics

From Faraday's and Biot-Savart's laws and assuming an ideal integrator on the sensor coil output voltage, the system dynamics write in the standard state-space form as

$$\begin{cases} \dot{\mathbf{x}} &= A\mathbf{x} + B\mathbf{u} + N\mathbf{v}_1 \\ \mathbf{z} &= M\mathbf{x} \\ \mathbf{y} &= C\mathbf{x} + \mathbf{v}_2 \end{cases} \qquad (2)$$

where $\mathbf{x} \in \mathbb{R}^{2N_mN_n}$ is the vector of MHD-modes b^r_{mn}, $\mathbf{u} \in \mathbb{R}^{N_u}$ is the active coil currents, $\mathbf{z} \subset \mathbf{x}$ is the optional performance vector channel and $\mathbf{y}$ denotes *time-integrated* sensor voltages, corresponding to a measure of mode $\mathbf{x}$ (time-averaged radial magnetic field). A, B, C, M and N are matrices of appropriate dimensions, $\mathbf{v}_1$ is an exogenous signal, further detailed in section II-C.2, and $\mathbf{v}_2$ is a white noise signal. State matrix elements are obtained from

$$\begin{aligned} A_{mn,m\prime n\prime} &\sim \gamma_{mn}\delta_{mn,m\prime n\prime} \\ B_{mn,ij} &\sim \tau^{-1}_{mn}\int_\Omega e^{-\iota(m\theta+n\phi)}\left(\hat{\mathbf{r}}\cdot\oint_{l_{ij}}\frac{\mathbf{dl}_{ij}\times(\mathbf{r}-\mathbf{r}_{ij})}{|\mathbf{r}-\mathbf{r}_{ij}|^3}\right)d\Omega \\ C_{pq,mn} &\sim \int_\Omega e^{+\iota(m\theta+n\phi)}f_{pq}A_{pq}d\Omega \end{aligned} \qquad (3)$$

where mn, ij and pq enumerate Fourier modes, active coils and sensor coils, respectively, and f_{pq}, A_{pq} are sensor coils aperture and area functions. The integration set Ω is a full period of the toroidal surface $(\theta,\phi) \in [-\pi,\pi[\times[-\pi,\pi[$.

In the following, state matrices in (2)-(3) are instantiated for T2R geometry and routing. Note that the consideration of both intrinsic field-errors and peripheral dynamics is imperative for simulating open- and closed-loop *shots*[2] [14], [3].

1) Modes coupling and aliasing of spatial frequencies: The finite spatial arrays of sensors and actuators fundamentally affect the transition from a single-mode to a multiple-mode model due to *aliasing*. It generally renders the sensors and actuators imprecise, and even introduce a bias. Aliasing also has an important impact on the closed-loop control, as a zero on the output *could* in reality be a combination of non-zero modes $\sum_{mn} \mathbf{b}_{mn}$, deceptively summing to a small number. The traditional IS regulator [6] consequently drives the output to zero but does so happily ignorant of individual mode amplitudes. This is a fairly recent appreciation of the need for further development of control systems for MHD experiments [15], [14]. Indeed, IS operation typically excites higher mode numbers, which are, supposedly, stable and mainly transient.

TABLE I
CHARACTERISTIC TIMES FOR CURRENT SETUP OF T2R.

Symbol	Value/order	Description/comment
τ_w	$\sim 10\,\mathrm{ms}$	Resistive wall time
τ_{mn}	$\lesssim \frac{1}{2}\tau_w$	Actual model mode time
τ_{MHD}	$\sim 1\mu\mathrm{s}$	Internal MHD activity/fluctuations
τ_d	$100\,\mu\mathrm{s}$	Digital sampling time, controller cycle
τ_h	$\sim 100\,\mu\mathrm{s}$	Control latency, dead time
τ_{CPU}	$< 100\,\mu\mathrm{s}$	Algorithm-dependent part of τ_h
τ_a	$8\,\mu\mathrm{s}$	Active amplifier first-order time
τ_c	$1\,\mathrm{ms}$	Active coil L/R-time
$\tau_{A\&D}$	$\sim 1\mu\mathrm{s}$	ADC/DAC settle, ns/μs respectively

2) Actuators dynamics, latencies and PID control: Consideration of the actuators dynamics and control latency is essential for a realistic description of the control problem, as detailed in [3]. Table I suggests[3] that we can consider a (lumped) active amplifier and an active coil model together with a dead-time τ_h in series with RWM dynamics. Using a first-order description, the system input $\mathbf{u}_{sys}(t)$ is inferred from the digital control signal $\mathbf{u}_{DAC}(t)$ through a relationship

$$\mathbf{u}_{sys}(t) \approx \frac{1}{\tau_c s+1}\frac{\kappa}{\tau_a s+1}\mathbf{u}_{DAC}(t-\tau_h) \qquad (4)$$

Introducing the system (A_ξ, B_ξ, C_ξ) to describe the previous dynamics, the resulting state-space matrices $(\bar{A}, \bar{B}, \bar{C})$ are obtained as

$$\bar{A} = \begin{pmatrix} A & BC_\xi \\ 0 & A_\xi \end{pmatrix},\ \bar{B} = \begin{pmatrix} 0 \\ B_\xi \end{pmatrix},\ \bar{C} = \begin{pmatrix} C & 0 \end{pmatrix}$$

The closed-loop dynamics, using a PID controller, is obtained as follows. The state considered is $\tilde{\mathbf{x}} = (\mathbf{x}^T\ \mathbf{q}^T)^T$, which includes the integrator state $\mathbf{q}(t) = \int_{-\infty}^{t}\mathbf{e}(\tau)d\tau$,

[2]One single experiment is known as a *shot*. Open- and closed-loop here specifically refers to RWMs.

[3]Neglecting $\tau_{A\&D}$ and quantization.

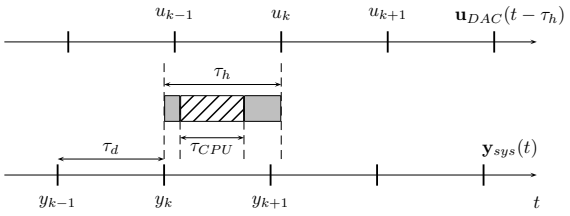

Fig. 2. Delay from control system. Note τ_h, dependent of control algorithm, possibly greater than τ_d but obviously $\tau_{CPU} < \tau_d$ for a working system. Sample frequency $f_s = 1/\tau_d$. Input y_k sampled from sensor coils, output u_k is the DAC-output subsequently fed to the active coil amplifiers as augmented system input.

where $e(t) = y(t)$ is the error (the reference is zero). Modeling the derivative action by finite time-difference renders the controller

$$\mathbf{u}_{DAC}(t) = K_p\mathbf{e}(t) + K_i\mathbf{q}(t) + \tau_d^{-1}K_d(\mathbf{e}(t) - \mathbf{e}(t-\tau_d))$$

The closed-loop dynamics is consequently obtained as

$$\begin{aligned}\dot{\tilde{\mathbf{x}}}(t) &= \mathcal{A}_0\tilde{\mathbf{x}}(t) + \mathcal{A}_1(\theta)\tilde{\mathbf{x}}(t-\tau_h) \\ &\quad + \mathcal{A}_2(\theta)\tilde{\mathbf{x}}(t-\tau_h-\tau_d) + \mathcal{E}\mathbf{v}_1(t) \qquad (5)\end{aligned}$$

where the control parameters $\theta = (K_p, K_i, K_d)$ enter affinely and

$$\begin{aligned}\mathcal{A}_0 &= \begin{pmatrix} \bar{A} & 0 \\ \bar{C} & 0 \end{pmatrix},\ \mathcal{A}_1(\theta) = \begin{pmatrix} \bar{B}(K_p + K_d/\tau_d)\bar{C} & \bar{B}K_i \\ 0 & 0 \end{pmatrix} \\ \mathcal{A}_2(\theta) &= \begin{pmatrix} \bar{B}(-K_d/\tau_d)\bar{C} & 0 \\ 0 & 0 \end{pmatrix},\ \mathcal{E} = \begin{pmatrix} \bar{N} \\ 0 \end{pmatrix}\end{aligned} \qquad (6)$$

Note that the gain matrices have a diagonal form $K_\eta = k_\eta I$, where k_η is a scalar and $\eta \in \{p, i, d\}$ for the IS scheme.

C. Open-loop error estimation and parameter identification

Here, see Fig. 1(c), an error field $\mathbf{v}_1$ estimate is obtained from experimental data via *model-based filtering* of open-loop (in the sense of RWM-control) shots, while actuators $G_{act}(s)$ are found by straighforward parametric identification. The controller cycle time τ_d is set at a nominal value $\tau_d = 100\,\mu\mathrm{s}$.

1) Actuators dynamics identification: In order to identify the actuator dynamics (4), we consider the transfer channels i: $u^{ij}_{DAC}(t) \mapsto u^{ij}_{sys}(t)$, for each experiment j. The amplifiers' time constants τ_a^{ij} are fixed and we identify the remaining parameters $\rho^{ij} \doteq \{\tau_c^{ij}, \tau_h^{ij}, \kappa^{ij}\}$. Following the approach presented in the previous section (MIMO model built from a set of SISO dynamics), we determine the optimal averaged model $\rho^* = \langle\langle \rho^{ij*}\rangle_i\rangle_j$. This model averages the optimal parameters $\rho^{ij*} = \arg\min_{\rho^{ij}} J^{ij}$ that minimize the error functional

$$J^2(\rho^{ij}) = \frac{1}{T}\int_0^T \left(u^{ij}_{sys}(\tau) - u^{ij}_{sim}(\tau, \rho^{ij})\right)^2 d\tau$$

where u_{sys} is the experimental data and u_{sim} is the model output, for each transfer channel.

A real-time PRBS (*pseudorandom binary sequence*) generator [16] was implemented to produce $64\times$ parallel SISO

identification inputs. This generator spent $\sim 5\,\mu$s per cycle of τ_{CPU} and can thus be considered to yield an identification of *minimum* latency. The optimal set of parameters $\rho^{ij\,*}$ is obtained by minimizing $J(\rho^{ij})$ with a *Quasi-Newton* method initialized from a nominal guess $\rho_0^{ij} = (1\text{ms},\, 100\mu\text{s},\, 4\text{A/V})$. The overall average model ρ^* was found to be $(\tau_c^*, \tau_h^*, \kappa^*) = (0.989\text{ms},\, 77.7\mu\text{s},\, 3.96\text{A/V})$ by residual minimization. A finite difference gradient approximations and a scaling of the decision variables to the order of unity led to a rapid convergence (1-14 iterations $\forall i,j$) of the numerical scheme.

The identification data set shows channel-by-channel variations and all the computations involving the *full* MIMO model (2) consequently use the individual channel averages $\langle \rho^{i,j} \rangle_j$, except for the time-delay, which is set identical for all channels. A worst-case τ_h (using maximum τ_{CPU}) exceeding $200\,\mu$s is consistent with recorded data for particular channels.

2) Error-field estimation and filtering: To estimate the error-field time-evolution, a set of open-loop shots are analyzed in the scope of model (2). A standard *Kalman Filter* (KF, e.g. [17]) is formed from (2) by adding *placeholder* states that represent the error-field $\tau_s \dot{\mathbf{x}}_s + \mathbf{x}_s = 0$. More precisely, the KF estimates the state vector for

$$\left\{ \begin{array}{rcl} \dot{\tilde{\mathbf{x}}} & = & \left(\begin{array}{cc} A & N \\ 0 & -\tau_s^{-1} I \end{array} \right) \tilde{\mathbf{x}} + \left(\begin{array}{c} B \\ 0 \end{array} \right) \mathbf{u} + \mathbf{v}_1' \\ \mathbf{y} & = & \left(\begin{array}{cc} C & 0 \end{array} \right) \tilde{\mathbf{x}} + \mathbf{v}_2 \end{array} \right. \tag{7}$$

where $\tilde{\mathbf{x}}(t) \doteq (\mathbf{x}(t)^T\, \mathbf{x}_s(t)^T)^T$, and $\mathbf{v}_1'$ and $\mathbf{v}_2$ are white noise. The filter takes $(\mathbf{u}(t)^T\, \mathbf{y}(t)^T)^T$ as inputs and outputs the state-estimate $\hat{\tilde{\mathbf{x}}} = (\hat{\mathbf{x}}^T(t)\, \hat{\mathbf{x}}_s^T(t))^T$. Note that the estimated error field $\hat{\mathbf{x}}_s(t)$ has a specific physical interpretation as it corresponds to a driving term for *inter alia* RWM-instabilities. The KF is tuned for very fast error-state $\hat{\mathbf{x}}_s$ due to the fact that an error in the growth-rate $\gamma_{mn}^{true} = \gamma_{mn}^{nominal} + \gamma_{mn}^{(1)}(t)$ affects in principle $\mathbf{v}_1$. This is expressed by the relation

$$\begin{aligned} \tau_{mn} \dot{b}_{mn}^r &= \tau_{mn} \left\{ \gamma_{mn} + \gamma_{mn}^{(1)}(t) \right\} b_{mn}^r + b_{mn}^{r,err} + b_{mn}^{r,act} \\ &= \tau_{mn} \gamma_{mn} b_{mn}^r + b_{mn,eff}^{r,err} + b_{mn}^{r,act} \end{aligned}$$

which implies that the *effective* error $b_{mn,eff}^{r,err} \equiv \tau_{mn} \gamma_{mn}^{(1)}(t) b_{mn}^r + b_{mn}^{r,err}$, associated with $\mathbf{v}_1$ in the model considered, depends on the mode amplitude itself. The discretized augmented model (7) is used for offline smoothing with the well-known *Rauch-Tung-Striebel* [17] forward-backward algorithm.

III. STABILITY ANALYSIS AND DELAY EFFECTS

Consider the (asymptotic) stability of the DDE-class (5). The corresponding characteristic equation of (5) reads as (for $n = 2$)

$$\det \Delta(s) = \det \left(sI - \mathcal{A}_0 - \sum_{i=1}^{n} \mathcal{A}_i e^{-s\tau_i} \right) = 0 \tag{8}$$

It is well-known that (8) has an *infinite* number of roots $s = \lambda_j$ and that (5) has a point spectrum. Furthermore, since the set $\{\lambda_j : \det \Delta(\lambda_j) = 0,\, \mathrm{Re}(\lambda_j) > a\}$ with a real is *finite* (see, e.g., [18] and the references therein), it follows that the stability problem is reduced to analyze the location of the *rightmost* characteristic roots with respect to the imaginary axis (see, for instance, [19] for numerical computations).

The continuity properties of the spectral abscissa with respect to the system parameters (including the delays) allows a better understanding of the effects induced by the parameters' change on the stability of the system. Without entering into details, such properties will be exploited in the sequel. For the sake of brevity, we will discuss some of the properties of our delay system without giving a complete characterization of the stability regions in the corresponding parameter space. This issue will be detailed in future works.

A. Mode-control and perfect decoupling; SISO dynamics

Consider here a fictitious situation where *perfect* actuators and sensors are available (in a no-aliasing sense; infinite array of vanishing-size coils). Ideally, we could then, according to (1), measure and affect each Fourier mode (m, n) independently, achieving perfect decoupling and effectively reducing the dynamics to a SISO system with actuator delay:

$$G_{mn}(s) = \frac{1}{\tau_{mn} s - \tau_{mn} \gamma_{mn}} \frac{1}{\tau_c s + 1} \frac{1}{\tau_a s + 1} e^{-s\tau_h} \tag{9}$$

readily converted to a closed-loop description (5) with $\mathcal{A}_i \in \mathbb{R}^{4\times 4}$. A static mode-control (MC) decoupling controller would typically be computed by taking SVD pseudoinverses of (3), and it can be demonstrated that doing this produce aliased side-bands on the inverse approximations [14]. IS operation, considered here is "far-from-perfect" mode-control, but the underlying SISO dynamics (1) is fundamentally important, and is considered a benchmark case. Fig. 3(a)

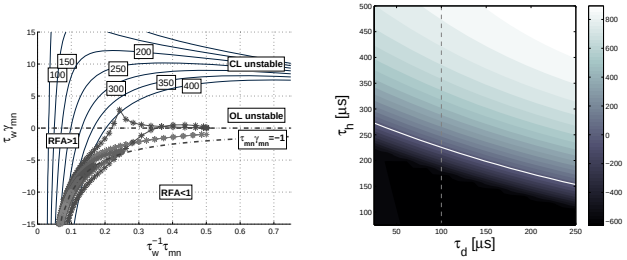

(a) Stability in RWM parameter space.

(b) SISO-set stability in (τ_h, τ_d)-space.

Fig. 3. Stability and time-delay impact on RWM dynamics.

shows stability contours ($\max_j \mathrm{Re}(\lambda_j) = 0$) for $\tau_h = \{100 - 400\mu\text{s}\}$ in RWM parameter space (τ, γ), for fixed PID gains[4] $\theta_{old} = (-10.4, -1040, -0.0026)$.

In Fig. 3(a) *Resonant-field amplification* (RFA) regions [13] are indicated, an effect related to the error-field, as modeled in (7).

[4]When *quoting numerical* gains: k_η correspond to dimensionless loop-gains (*negative*), related to (*positive*) experiment settings $k_\eta = \beta K_\eta$ [3], with a nominal conversion factor $\beta = -6.5 \times 10^{-2}$.

B. Spectrum dependence on τ_h; MIMO and SISO cases

We now consider the dependence of the spectral abscissa with respect to the parameter τ_h. This is done by fixing the gains $(K_p, K_i, K_d) = (146, 57000, 0.085)$ and the delay $\tau_d = 100\mu$s for IS operation on full MIMO model (5). The impact of the delay τ_h is thereby highlighted for a given set of parameters. Computing the rightmost closed-loop roots, critical crossing of the imaginary axis occurs at $\tau_h \approx 201\mu$s. This can be compared with the SISO analog, Fig. 3(b), where instability occurs at $\tau_h \approx 225\mu$s. The set of modes was in both cases $\mathcal{K} = \{1,3\} \times \{-24, \ldots, +23\}$. In conclusion, multivariable effects are *not* negligible.

IV. MODEL-BASED CONTROL AND DELAY COMPENSATION

Our aim is to select PID gains for DDE (5) that ensure stability and minimize the closed-loop spectral abscissa. The PID in the actual experiment control system (IS) is regarded as fixed, imposing a structural constraint on the optimization problem. A fixed-order/fixed-structure controller synthesis approach is utilized to find gains for T2R IS operation. The method, as instantiated in this work, concerns model (5), i.e. it handles time-delays explicitly, which has a significant practical benefit: developing control algorithms with varying computational complexity (varying τ_{CPU}) implies varying τ_h, which can be accounted for.

It is recognized that other widely spread iterative tuning techniques such as [20] also could be applied for this particular problem. This is subject for the sequel.

A. Direct eigenvalue optimization (DEO)

The asymptotic damping maximization of (5) is formulated as minimizing the spectral abscissa of the characteristic equation [18] with

$$\theta^* = \arg\min_{\theta} \max_{\lambda} \{\mathrm{Re}\,(\lambda) : \det \Delta(\lambda, \theta) = 0\}$$

This problem is generally both nonconvex and nonsmooth, which motivates a hybrid SISO/MIMO method. The general MIMO problem size (5) is typically large; e.g. a set $(m,n) \in \mathcal{K} = \mathcal{M} \times \mathcal{N} = \{1,3\} \times \{-16, \ldots, +15\}$ results in $\mathcal{A}_i \in \mathbb{R}^{384\times 384}$. However, for IS, each coil measures a linear combination of fundamental dynamics (1) over $\mathcal{K}$, but does not discriminate between modes. This relates to the previously discussed hypothesis that the MIMO model can be approximated by a set of SISO systems. The MIMO optimization problem is then approximated to the problem of minimizing the maximum SISO spectral abscissas over $\mathcal{K}$ with

$$\tilde{\theta}^* = \arg\min_{\theta} \max_{k\in\mathcal{K}} \max_{\lambda} \{\mathrm{Re}\,(\lambda) : \det \Delta_k(\lambda, \theta) = 0\} \quad (10)$$

where Δ_k denotes the characteristic matrix ($\in \mathbb{R}^{4\times 4}$) for (5) for a single mode $k = (m,n)$. We employ the recently developed *gradient-sampling* (GS) method [21], a *robustified* steepest-descent method suitable for nonsmooth optimization, to solve (10) using finite difference gradient approximations.

We investigate two different parameterizations of the controller, implicitly assigning the closed-loop performance and control-input norm, respectively by:

a) varying k_p and searching for the optimal $\tilde{\theta}^* = (k_i^*, k_d^*)$ for a nominal τ_h, and

b) varying τ_h and determining the full optimal PID $\tilde{\theta}^* = (k_p^*, k_i^*, k_d^*)$.

The mode-sets are considered for $a) - b)$ were $\mathcal{K}_1 = \{1,3\}\times\{-16, \ldots, +15\}$ and $\mathcal{K}_2 = \{1,3\}\times\{-24, \ldots, +23\}$ respectively. In *a)* $\tau_h = 77.7\mu$s, which corresponds to the *minimum* actuator latency.

B. Optimization results

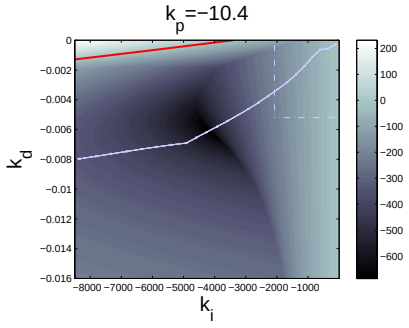

Fig. 4. Closed-loop spectrum optimization.

Gain design strategy $a)$, where the optimal (k_i^*, k_d^*) are obtained with preset values of k_p and τ_h, is illustrated in Fig. 4, which depicts the rightmost values of the closed-loop spectrum for a fixed k_p in (k_i, k_d)-space (the optimum corresponding to the darkest region). The bold dotted line corresponds to the evolution of (k_i^*, k_d^*) when k_p varies (going left when the magnitude of k_p is increased). The red line in the upper left corner is the stability boundary and the rectangle in upper-right corner is the region of uniformly randomized initializations for the GS method.

Comparable numerical values were obtained for gain design strategy $b)$. A few optimal settings are seen in table II. For $b)$ the minimum objective value is increased (spectral abscissa traveling rightwards) as the time-delay increases, as expected.

The optimization algorithm was numerically robust on problems $a), b)$. All runs converged, normally within $10-30$ iterations, from randomized starting controllers. Multiple runs were taken for each controller, yielding identical results (within reasonable numerical accuracy).

V. EXPERIMENTAL RESULTS

The new control approach presented in the previous sections motivated new series of experiments on T2R: shot numbers $\#20743 - \#20755$ and $\#20824 - \#20838$. Experimental plasma equilibrium conditions were set with a toroidal plasma current $I_p \approx 85\,\mathrm{kA}$, a shot length $\tau_p =\sim 50 - 70\,\mathrm{ms}$ and *reversal* and *pinch* parameter values (typically used to characterize RFP equilibria [8]) $(F, \Theta) \approx (-0.27, 1.72)$.

TABLE II

T2R EXPERIMENTAL RESULTS.

$[J_y] = (\mathrm{mT})^2 \times 10^{-3}$, $[J_u] = (\mathrm{A})^2 \times 10^3$.

Shot#	K_p	K_i	K_d	J_y	J_u	Remark
20743	150	16000	0.05	1.04	1.66	old gain 1
20744	160	16000	0.04	1.14	1.80	old gain 2
20746	106	37500	0.061	0.581	2.12	series *a)*
20747	126	47500	0.073	0.808	1.94	*a)*
20827	150	16000	0.05	1.12	1.60	old gain 1
20833	119.6	46800	0.065	0.680	1.77	*b)*
20835	106.8	39860	0.058	0.645	1.64	*b)*

We only consider strict IS performance in terms of plant output, and introduce a suitable scalar measure to compare experimental (and simulated) performance.

A. Generic measure of experimental performance

The overall controller performance is summarized with the general quadratic measure

$$J_x(\tilde{\theta}) \equiv \frac{1}{t_1 - t_0} \int_{t_0}^{t_1} \mathbf{x}^T(\tau, \tilde{\theta}) Q_x \mathbf{x}(\tau, \tilde{\theta}) d\tau \qquad (11)$$

where $\mathbf{x} = \mathbf{y}_{sys}$ or $\mathbf{u}_{sys}$, and $\tilde{\theta}$ the controller setting. We do not consider any specific channel weighting ($Q_y = Q_u = I \in \mathbb{R}^{64\times 64}$) and the integral is approximated by trapezoidal summation of non-filtered sampled data. The nature of T2R shots [3] suggests a split of the timespan $[t_0, t_1]$ into two parts, corresponding to the *transient* (first $10\,\mathrm{ms}$) and *steady-state* behaviors (between 10 and $\sim 50\,\mathrm{ms}$).

B. Performance improvements

The performance improvements are summarized in Table II for the *steady-state* interval $10-45\mathrm{ms}$, using cost function (11). The optimized controllers $a)$ and $b)$ clearly reveal a significant 44% $(1 - 0.581/1.04)$ reduction of average field energy at the sensors during steady-state period. This is at the expense of a higher input power, increased by 28% $(2.12/1.66 - 1)$. Furthermore, simulations with the MIMO model, as driven by the identified $\mathbf{v}_1$ of section II-C.2, reveal that the *old PID coefficients are significantly suboptimal* in both full model (2) and experiment compared to the new PID coefficients.

VI. CONCLUSIONS

A new model for MHD instabilities in T2R, explicitly including important geometrical and engineering aspects was presented. Direct closed-loop PID gain optimization for the corresponding DDE model was shown to provide useful results for experimental IS feedback in a RFP fusion research device. Simulations and experiments for the T2R device have shown some qualitative agreement, further indicating the applicability of the model to real experimental conditions. In short, results strongly encourage future work, theoretically and experimentally, in both physical modeling and multivariable control.

ACKNOWLEDGEMENTS

The authors acknowledge support from the EURATOM fusion research programme through the contract of association EURATOM-VR, and wish to express appreciation for reviewers' comments helping to improve the manuscript.

REFERENCES

[1] M. Walker *et al.*, "Emerging applications in tokamak plasma control: Control solutions for next generation tokamaks," *IEEE Control System Magazine*, vol. 26, pp. 35–63, 2006.

[2] M. Shimada *et al.*, "Progress in the ITER physics basis, chapter 1: Overview and summary," *Nuclear Fusion*, vol. 47, no. 6, pp. S1–S17, 2007. [Online]. Available: http://stacks.iop.org/0029-5515/47/S1

[3] P. R. Brunsell, K. E. J. Olofsson, L. Frassinetti, and J. R. Drake, "Resistive wall mode feedback control in EXTRAP T2R with improved steady-state error and transient response," *Physics of Plasmas*, vol. 14, no. 10, p. 102505, 2007. [Online]. Available: http://link.aip.org/link/?PHP/14/102505/1

[4] D. Yadikin, "Resistive wall mode stability and control in the reversed-field pinch," Doctoral Thesis, KTH Electrical Engineering, Stockholm, Sweden, 2006.

[5] P. R. Brunsell *et al.*, "Feedback stabilization of multiple resistive wall modes," *Physical Review Letters*, vol. 93, no. 22, p. 225001, 2004. [Online]. Available: http://link.aps.org/abstract/PRL/v93/e225001

[6] C. Bishop, "An intelligent shell for the toroidal pinch," *Plasma Physics and Controlled Fusion*, vol. 31, no. 7, pp. 1179–1189, 1989. [Online]. Available: http://stacks.iop.org/0741-3335/31/1179

[7] J. Wesson, *Tokamaks*, 3^{rd} ed., ser. International Series of Monographs on Physics. New York: Oxford Science Publications, 2004, no. 118.

[8] J. Freidberg, *Ideal Magnetohydrodynamics*. Plenum Press, 1987.

[9] P. Davidson, *An Introduction to Magnetohydrodynamics*. Cambridge University Press, 2001.

[10] P. R. Brunsell, J.-A. Malmberg, D. Yadikin, and M. Cecconello, "Resistive wall modes in the EXTRAP T2R reversed-field pinch," *Physics of Plasmas*, vol. 10, no. 10, pp. 3823–3833, 2003. [Online]. Available: http://link.aip.org/link/?PHP/10/3823/1

[11] R. Fitzpatrick and E. P. Yu, "Feedback stabilization of resistive shell modes in a reversed field pinch," *Physics of Plasmas*, vol. 6, no. 9, pp. 3536–3547, 1999. [Online]. Available: http://link.aip.org/link/?PHP/6/3536/1

[12] R. Fitzpatrick, E. Rossi, and E. P. Yu, "Improved evolution equations for magnetic island chains in toroidal pinch plasmas subject to externally applied resonant magnetic perturbations," *Physics of Plasmas*, vol. 8, no. 10, pp. 4489–4500, 2001. [Online]. Available: http://link.aip.org/link/?PHP/8/4489/1

[13] D. Gregoratto *et al.*, "Studies on the response of resistive-wall modes to applied magnetic perturbations in the EXTRAP T2R reversed field pinch," *Physics of Plasmas*, vol. 12, no. 9, p. 092510, 2005. [Online]. Available: http://link.aip.org/link/?PHP/12/092510/1

[14] E. Olofsson, "Modelling and design for active control of magnetohydrodynamic unstable modes in EXTRAP T2R," Master's thesis, Royal Institute of Technology (KTH), Jan. 2007.

[15] P. Zanca, L. Marrelli, G. Manduchi, and G. Marchiori, "Beyond the intelligent shell concept: the clean-mode-control," *Nuclear Fusion*, vol. 47, no. 11, pp. 1425–1436, 2007. [Online]. Available: http://stacks.iop.org/0029-5515/47/1425

[16] L. Ljung, *System Identification - theory for the user*, 2^{nd} ed. Prentice-Hall, 1999.

[17] F. Gustafsson, *Adaptive filtering and change detection*. John Wiley & Sons Ltd., 2000.

[18] W. Michiels and S.-I. Niculescu, *Stability and Stabilization of Time-Delay Systems: An Eigenvalue-Based Approach*, ser. Advances in Design and Control. SIAM, 2007, vol. 12.

[19] K. Engelborghs, "DDE-BIFTOOL: a matlab package for bifurcation analysis of delay differential equations," 2000. [Online]. Available: citeseer.ist.psu.edu/engelborghs00ddebiftool.html

[20] M. Killingsworth, N.J.; Krstic, "PID tuning using extremum seeking: online, model-free performance optimization," *Control Systems Magazine, IEEE*, vol. 26, no. 1, pp. 70–79, Feb. 2006.

[21] J. V. Burke, A. S. Lewis, and M. L. Overton, "A robust gradient sampling algorithm for nonsmooth, nonconvex optimization," *SIAM Journal on Optimization*, vol. 15, no. 3, pp. 751–779, 2005. [Online]. Available: http://link.aip.org/link/?SJE/15/751/1